

ToddlerBot: Open-Source ML-Compatible Humanoid Platform for Loco-Manipulation

Haochen Shi* Weizhuo Wang* Shuran Song† C. Karen Liu†

*Equal contribution †Equal advising
Stanford University

<https://toddlerbot.github.io>

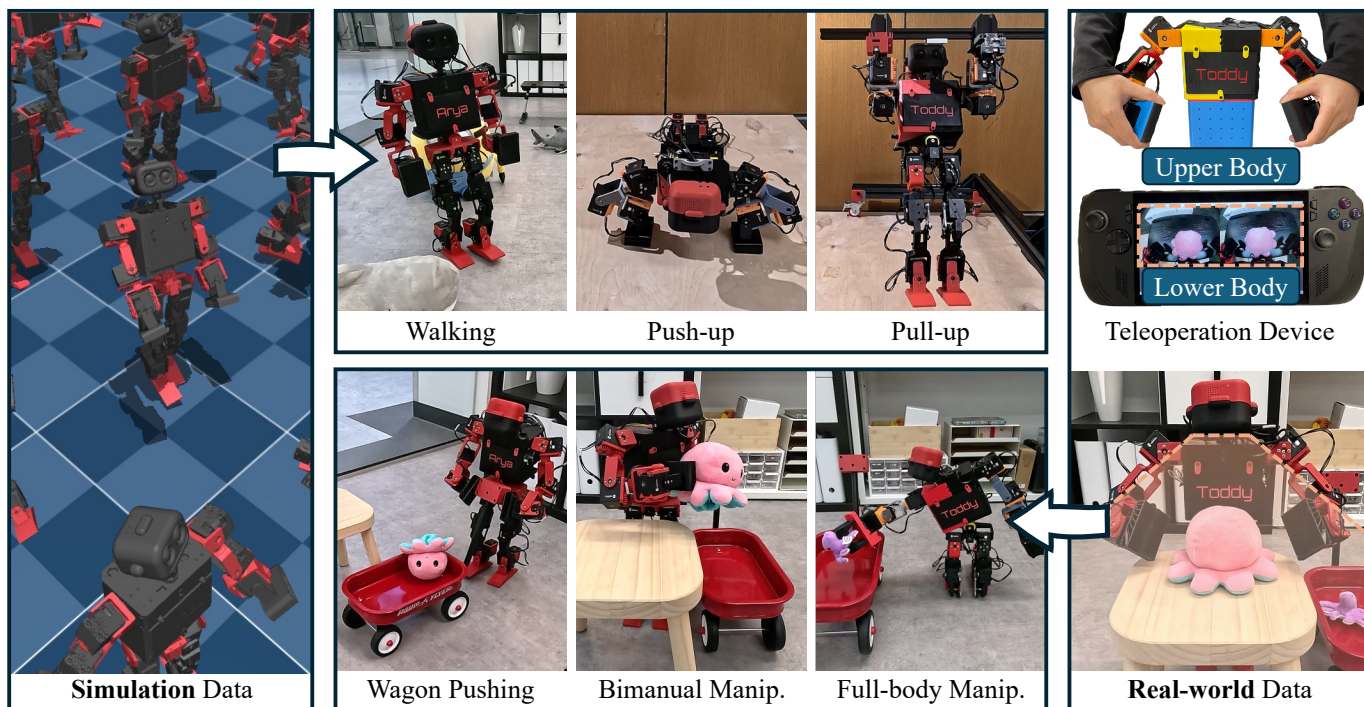


Figure 1: **ToddlerBot** is an open-source, ML-compatible humanoid platform for efficiently collecting large-scale, high-quality training data in both simulation and the real world. We leverage massive parallel environments, an accurate digital twin for simulation, and an intuitive teleoperation device for precise upper and lower body control in real-world data collection. We demonstrate that ToddlerBot meets these requirements and successfully acquires a diverse set of loco-manipulation skills from both data sources, including walking, push-ups, pull-ups, wagon pushing, bimanual, and full-body manipulation.

Abstract—Learning-based robotics research driven by data demands a new approach to robot hardware design—one that serves as both a platform for policy execution and a tool for embodied data collection to train policies. We introduce ToddlerBot, a low-cost, open-source humanoid robot platform designed for scalable policy learning and research in robotics and AI. ToddlerBot enables seamless acquisition of high-quality simulation and real-world data. The plug-and-play zero-point calibration and transferable motor system identification ensure a high-fidelity digital twin, enabling zero-shot policy transfer from simulation to the real-world. A user-friendly teleoperation interface facilitates streamlined real-world data collection for learning motor skills from human demonstrations. Utilizing its data collection ability and anthropomorphic design, ToddlerBot is an ideal platform to perform whole-body loco-manipulation. Additionally, ToddlerBot’s compact size (0.56 m, 3.4 kg) ensures safe operation in real-world environments. Reproducibility is achieved with an entirely 3D-printed, open-source design and

commercially available components, keeping the total cost under 6000 USD. Comprehensive documentation allows assembly and maintenance with basic technical expertise, as validated by a successful independent replication of the system. We demonstrate ToddlerBot’s capabilities through arm span, payload, endurance tests, loco-manipulation tasks, and a collaborative long-horizon scenario where two robots tidy a toy session together. By advancing ML-compatibility, capability, and reproducibility, ToddlerBot provides a robust platform for scalable learning and dynamic policy execution in robotics research.

I. INTRODUCTION

Conventional robot design prioritizes factors such as actuator strength, sensor accuracy, mechanical precision, and repeatability—key objectives for developing robust control algorithms. However, these platforms are not inherently aligned with modern robot learning paradigms driven by embodied

Table I: Comparison with Other Humanoid Research Platforms.

Humanoid	Size(m)	Weight(kg)	# Active DoFs ^(a)	Manipulation	Locomotion	Sim Data	Real Data	Open Source	Price(\$)
BD Atlas [8]	1.50	89.0	28	✓	✓	-	-	✗	-
Berkeley [27]	0.85	16.0	12	✗	✓	✓	✗	code	10K
Booster T1 [35]	1.18	30.0	23	✓	✓	✓	✗	code	34K
BRUCE [28]	0.70	4.8	16	✗	✓	✓	✗	code	6.5K
Cassie [33]	1.15	35.0	10	✗	✓	✓	✗	code	250K
Digit [34]	1.75	65.0	16	✓	✓	✓	✗	code	250K
Duke [49]	1.00	30.0	10	✗	✓	✓	✗	everything	16K
Figure [9]	1.68	70.0	26	✓	✓	-	-	✗	-
Fourier GR1 [10]	1.65	55.0	32	✓	✓	-	-	✗	110K
iCub [32]	1.04	24.0	32	✓	✓	✓	✗	code	300K
MIT [5]	1.04	24.0	18	✗	✓	-	-	✗	-
NAO H25 [31]	0.57	5.2	23	✓	✓	✓	✗	code	14K
Optimus [44]	1.73	57.0	28	✓	✓	-	-	✗	-
Robotis OP3 [36]	0.51	3.5	20	✗	✓	✓	✗	code	11K
Unitree G1 [47]	1.32	35.0	29	✓	✓	✓	✓	code	57K
Unitree H1 [46]	1.76	47.0	19	✓	✓	✓	✓	code	70K
Ours	0.56	3.4	30	✓	✓	✓	✓	everything ^(b)	6K
Average Adult [14]	1.73	70.9	32 ^(c)	✓	✓	-	-	-	-

^(a) The active degrees of freedom actuated by motors, excluding end effectors such as parallel grippers or dexterous hands.

^(b) Everything includes the digital twin, learning algorithms, hardware design, assembly manual, detailed documentation, and tutorials.

^(c) While human body is powered by over 600 muscles in reality, the primary functional movements of the human body can be approximated using 32 revolute joints: six DoFs per leg, seven DoFs per arm, three DoFs for the waist, and three DoFs for the neck, excluding fingers and toes.

data. A robot platform compatible with a machine learning (ML) approach must possess the innate ability to collect observation and action data seamlessly, both in simulation and in the real world, as these complementary data sources are essential for scalable policy learning. Simulation enables rapid and scalable data collection but relies heavily on accurate physics models. In contrast, real-world data tend to be more reliable but are often difficult to scale due to cost and safety concerns.

While some recent quadrupeds [23, 24] and robotic manipulators [50, 48, 41, 38, 2] have been designed with ML-compatibility in mind, we introduce **ToddlerBot, a humanoid robot platform** for robotics and AI research community (Figure 1), specifically developed to facilitate policy learning for both locomotion and manipulation skills. ToddlerBot is designed to maximize ML-compatibility, capability, and reproducibility, while minimizing the expertise and costs required for its construction and maintenance.

To address the need for ML-compatibility, ToddlerBot is designed not only to execute policies but also to serve as a robust data collection platform. It enables the acquisition of **high-quality simulation data** through a plug-and-play zero-point calibration procedure and transferable motor system identification (sysID) results. These tools ensure a high-fidelity digital twin without the need for additional tuning. We validate the quality of simulation data with both keyframe-interpolated motions (e.g., push-ups and pull-ups) and reinforcement learning (RL) policies (e.g., walking and turning), demonstrating the capability for zero-shot sim-to-real transfer. ToddlerBot can also acquire **scalable real-world data**. We design an intuitive teleoperation interface that allows simultaneous control of ToddlerBot’s upper and lower body to collect whole-body manipulation data and develop effective visuomotor policies. Additionally, ToddlerBot’s small size and

weight (0.56 m, 3.4 kg) ensure safe and accessible operation in real-world environments.

Beyond ML-compatibility, ToddlerBot is designed with a focus on capability and reproducibility. A humanoid has the potential to utilize scalable human demonstrations by leveraging its anatomical similarity to the human body. As such, ToddlerBot features an anthropomorphic design with 30 active degrees of freedom (excluding end effectors), powered by carefully selected motors comparable to human muscle strengths normalized by the body size. We demonstrate ToddlerBot’s capabilities through arm span, payload, and endurance tests and various open-loop and closed-loop locomanipulation tasks.

Reproducibility is achieved through low-cost, open-source designs and readily accessible hardware components. ToddlerBot uses commercially available motors and is completely 3D-printed, with a total cost under 6,000 USD (90% of the cost is for motors and computers). We will release digital twin software, learning algorithms, hardware designs, and comprehensive tutorials to ensure that ToddlerBot can be built at home with basic knowledge of hardware and software, without requiring specialized equipment for manufacturing or repair. To validate reproducibility, we enlisted a CS-major student who is not involved in this project to independently build another instance of ToddlerBot with the provided assembly manual and successfully zero-shot transferred locomanipulation policies between the two instances. Finally, we showcase a collaborative long-horizon task in which two ToddlerBot robots work together to tidy a room by organizing stuffed toys from a table and the floor.

II. RELATED WORKS

In recent years, numerous humanoid robots have been developed, showcasing diverse designs and capabilities. Industrial humanoids such as Boston Dynamics Atlas [8], Booster

T1 [35], Cassie [33], Digit [34], Figure [9], Fourier GR1 [10], NAO H25 [31], Tesla Optimus [44], Robotis OP3 [36], Unitree G1 [47], and H1 [46] demonstrate remarkable technological advancements. On the other hand, humanoids from research institutions, including the Berkeley Humanoid [27], BRUCE [28], Duke Humanoid [49], iCub [32], and MIT Humanoid [5], also explore the humanoid design space with different emphasis. Humanoid robots can be evaluated using various metrics; we prioritize three core attributes: ML-compatibility, capability, and reproducibility. As outlined in Table I, we identify nine metrics to compare these attributes across different humanoid platforms.

Size and weight are critical factors when designing humanoid robots. A smaller humanoid is inherently cheaper, easier to build and repair, and safer. Larger, full-size humanoids typically require a substantial engineering team for operation and maintenance, along with specialized facilities like gantry cranes for safety. In contrast, smaller humanoids can be deployed by a small team, often a single person, and operated in constrained environments with simply a laptop. But what is the trade-off with a smaller size? Reduced size can limit a robot’s ability to manipulate human-scale objects, However, miniature humanoids can still effectively perform meaningful manipulation tasks when paired with appropriately scaled objects. Furthermore, learning to manipulate smaller objects and developing dynamic whole-body control and locomotion techniques are likely transferable to larger humanoids.

We argue that the number of active DoFs is crucial for the research value of a humanoid platform since more DoFs enable more human-like motion. While the human musculoskeletal system employs over 600 muscles working in complex synergies, the primary functional movements of the human body can be approximated using 32 revolute joints in a robotic system: six DoFs per leg, seven DoFs per arm, three DoFs for the waist, and three DoFs for the neck, excluding fingers and toes. Therefore, humanoid designs aim to achieve a DoF count as close to 32 as possible. The passive DoFs are less important as they do not contribute to the action space. We believe that the public perceived limited performance of miniature humanoids is primarily due to fewer DoFs. This limitation often arises from space constraints that restrict the incorporation of many DoFs, a challenge we have successfully addressed in ToddlerBot.

To qualitatively assess the capability, we evaluate the humanoid’s ability to perform both manipulation and locomotion tasks. While each type of motion is important, the combination of both is particularly compelling, as it unlocks opportunities for whole-body control research [19, 20, 12, 22, 29]. Furthermore, certain motions, such as push-ups, pull-ups, and cartwheels, go beyond traditional categories of manipulation and locomotion, treating them as prerequisites and requiring coordinated use of both arms and legs.

Recent advances show that large-scale simulation-based data collection is highly effective for locomotion [39, 42, 26], while real-world data collection is more promising for manipulation [6, 25, 30]. Therefore, an ideal humanoid research plat-

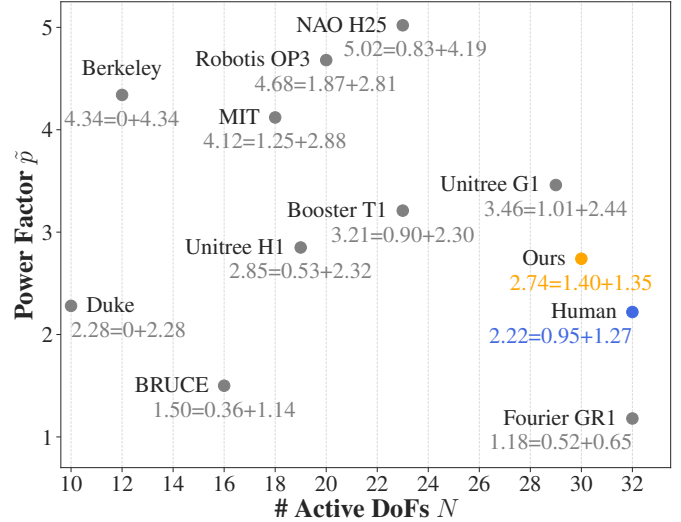


Figure 2: **Humanoid Metrics.** Two key criteria of humanoid capability are the number of active DoFs and power factor \tilde{p} (Equation 1). The total power factor is the sum of the upper and lower body power factor: $\tilde{p}_{total} = \tilde{p}_{upper} + \tilde{p}_{lower}$. ToddlerBot is the closest to human compared with other humanoids, implying potentially comparable loco-manipulation capabilities.

form should facilitate data collection in both simulation and real-world settings, which we defined as **ML-compatibility**.

Moreover, being open-source and low-cost is essential for others to reproduce. Without these qualities, research in this field would remain restricted to those with specialized expertise and significant resources. While making no compromise in functionality, ToddlerBot stands out as completely open-source and the most affordable among recent humanoid platforms, making it accessible to a wider range of researchers.

III. SYSTEM DESIGN

When designing humanoids, numerous factors must be considered, including payload, endurance, repeatability, degrees of freedom, cost, locomotion, and manipulation capabilities. Given this vast design space, ToddlerBot’s key design principles prioritize reproducibility, capability, and ML-compatibility. Unlike most prior works, we treat reproducibility as a hard constraint to narrow the design space, as our humanoid platform holds no value if it cannot be reproduced by others. With this assumption, we optimize the hardware for capability and enhance ML-compatibility through the careful design of the digital twin and teleoperation device.

A. Reproducibility - A Hard Constraint

We define reproducibility as the ability of a single person to replicate the robot system at home without specialized equipment. Limited access to manpower and facilities presents several challenges, including fabrication, space, and cost.

Fabrication. 3D printing has become a popular method for reproducing open-source hardware systems due to its accessibility and fast turnaround time [24, 41, 48]. Despite these merits, a key challenge is to ensure that printed parts are strong

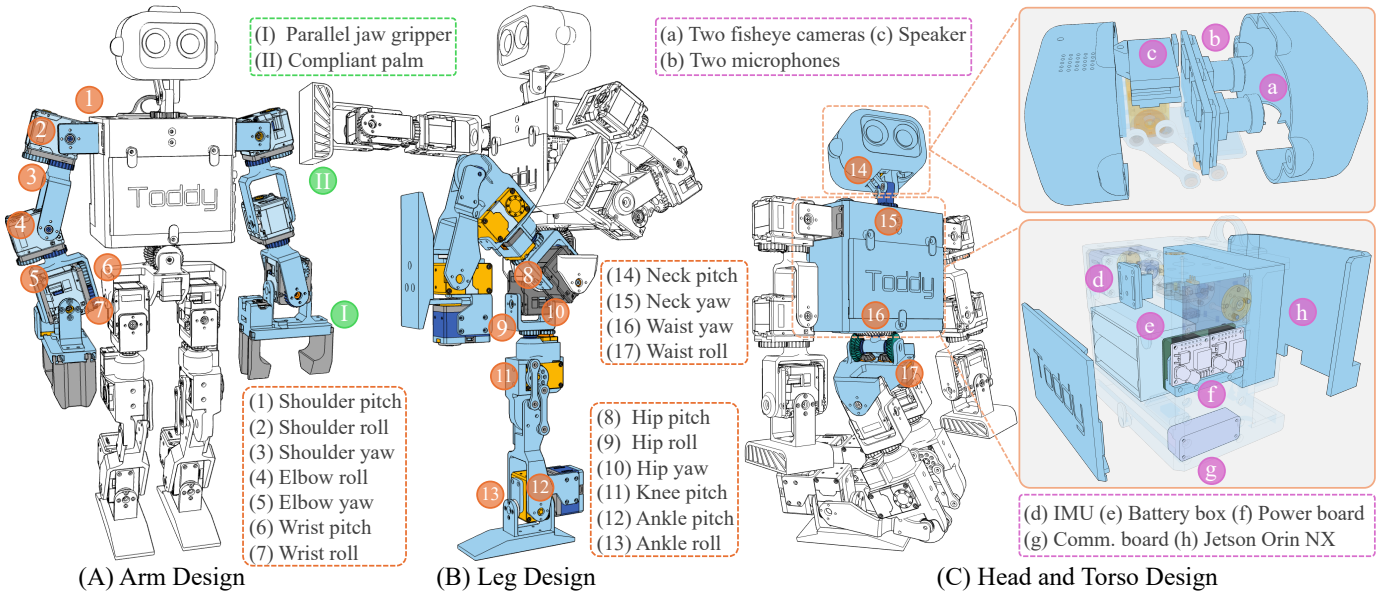


Figure 3: **Mechatronic Design.** We present three main sections: arm, leg, and head plus torso. We highlight ToddlerBot’s 30 active DoFs with orange markers: 7 DoFs per arm, 6 DoFs per leg, a 2-DoF neck, and a 2-DoF waist. Green markers indicate two end-effector designs—a compliant palm and a parallel-jaw gripper. Purple markers denote the sensor and electronics layout with exploded views, featuring two fisheye cameras, a speaker, two microphones, an IMU, and a Jetson Orin NX computer.

enough for a humanoid robot. We find that PLA suits most parts, while high-strength components can be reinforced with a stronger printing profile and carbon fiber-blended filaments. To ensure ease of assembly and maintenance, we detail our design considerations in Section VIII-A of the supplementary material. For non-3D-printable components, such as motors, we limit ourselves to readily available off-the-shelf items.

Space. In a home environment without equipment to ensure safety, it is essential to minimize the robot’s size. However, the robot’s size is constrained by the onboard computer required for policy execution. We use the NVIDIA Jetson Orin NX for AI model execution, and to fit both the computer and battery within the torso while maintaining human-like proportions, the robot’s height is capped at approximately 0.6 m.

Cost. With 3D printing, the total BOM cost of ToddlerBot is 6000 USD, with 90% spent on the computers and motors.

B. Capability - Design Objective

To quantitatively assess a humanoid robot’s capability, we propose two key metrics: power factor and the number of active DoFs. The power factor is defined as:

$$\tilde{p} = \frac{\sum_{i=0}^N |\tau_i^{\max}|}{h \cdot mg}, \quad (1)$$

where N denotes the number of active DoFs, $|\tau_i^{\max}|$ represents the peak torque of the i -th joint motor, h denotes the humanoid’s height, and mg represents the weight. We define \tilde{p} as the power factor, representing the total torque (and thus mechanical power) a robot can generate relative to its weight and height scale. A detailed discussion of this metric is provided in Section VIII-B of the supplementary material.

Intuitively, having a higher \tilde{p} means that a humanoid can perform energetic, dynamic motions more easily. We argue that \tilde{p} should at least exceed the human threshold \tilde{p}_{human} to achieve human-like motion, given the inherent gap between robot and human policies, assuming humans operate as an oracle policy that is energy efficient. However, raising \tilde{p} far beyond \tilde{p}_{human} can have adverse effects: it may lead to unnatural motion, excessive reliance on motor power, fewer DoFs to accommodate larger motors, reduced battery life, and increased safety concerns. Thus, pushing \tilde{p} past diminishing returns involves a practical trade-off. As shown in Figure 2, ToddlerBot has a \tilde{p} score closest to humans.

Mechatronic Design. As shown in Figure 3, ToddlerBot replicates the structure of an adult human body to maximize the number of active DoFs, enabling human-like motion and versatile loco-manipulation tasks. Each arm features seven DoFs with spur gears for axis-aligned transmission, ensuring high functionality and reachability. Each leg has six DoFs: three at the hip for a wide range of motion and optimized walking strides, a parallel linkage at the knee to reduce inertia, and two at the ankle for stable locomotion. The neck, with two DoFs, incorporates parallel linkages at the pitch joint for a compact design, allowing expressive motion and full head mobility. The waist, also with two DoFs, uses coupled bevel gears to balance the space budget and effectively transmit power from two motors for yaw and roll actuation, which enables whole-body control. Additionally, ToddlerBot offers two end-effector designs: a parallel jaw gripper for grasping and a compliant palm for tasks requiring a palm-like posture. The end-effector designs can be switched quickly within two minutes by removing a few screws.

For each active DoF, we maximize the range of mo-

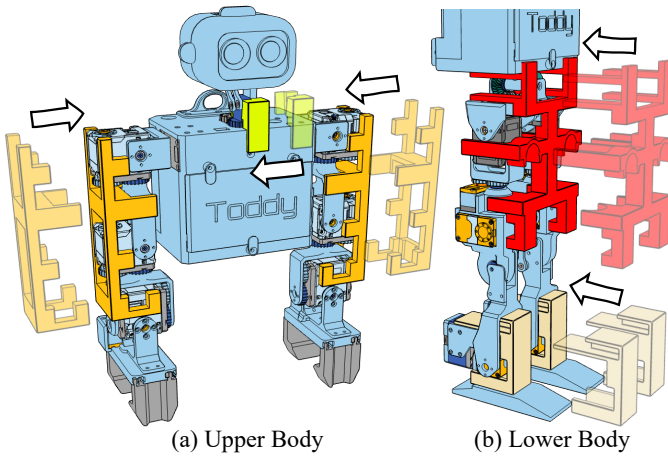


Figure 4: **Zero-point Calibration.** We 3D-print devices for the plug-and-play zero-point calibration procedure: orange for the arm, yellow for the neck, red for the hip, and beige for the ankle. Arrows indicate the insertion direction, and the zero-point is fixed once the devices click into place.

tion by optimizing geometries to prevent self-collisions as shown in Section VIII-C of the supplementary material. To address additional concerns such as space constraints, axis alignment, and inertia reduction, we integrate three primary transmission mechanisms in the mechanical design: spur gears, coupled bevel gears, and parallel linkages, as discussed in Section VIII-D of the supplementary material.

Motor Selection. We choose Dynamixel motors because of their robustness, reliability, and accessibility. Different types of Dynamixel motors were selected for various joints based on space constraints, torque requirements, and cost considerations. In terms of communication speed, Dynamixel motors communicate via a 5V TTL protocol running at 2M baudrate, providing full-state feedback for all 30 motors at 50 Hz using an off-the-shelf communication board. More detailed considerations are discussed in Section VIII-E of the supplementary material.

Sensors, Compute, and Power. To enhance ToddlerBot’s capabilities, we integrate a comprehensive set of sensors and computational components. Two fisheye cameras are included to expand the field of view, improving situational awareness. An Inertial Measurement Unit (IMU) is placed in the chest to provide state feedback for precise control. A speaker and microphones facilitate seamless communication with humans and other ToddlerBot instances. We provide a conversation example between two ToddlerBot instances in the supplementary video. The onboard computation is powered by a Jetson Orin NX 16GB, enabling real-time inference of machine learning models. Power management is handled by a custom-designed power distribution board with dual 12V converters. This system efficiently regulates the 12V rail and distributes power to various components, meeting the high energy demands while fitting within the limited space of the torso. The power budget is discussed in Section VIII-F of the supplementary material.

C. ML-Compatibility - Design Objective

Digital Twin. A high-fidelity digital twin is essential for high-quality simulation data collection and thus zero-shot sim-to-real transfer. We divide the digital twin development into two key components: zero-point calibration for correct kinematics and motor system identification for accurate dynamics.

Since Dynamixel motors lack an inherent zero point, a reliable method is needed to recalibrate after assembly, which is frequent during repairs or design iterations. As shown in Figure 4, we design calibration devices in CAD that quickly align the robot to its zero point, defined as standing with both arms besides the body. The process takes less than a minute.

With kinematics correctly calibrated, the next challenge is accurately identifying dynamics parameters. Firstly, while it may seem trivial, it is essential to carefully weigh all components to ensure an accurate weight distribution for the robot. Inspired by Haarnoja et al. [17], we collect sysID data by commanding the motors to track a chirp signal and use the resulting position tracking data to fit an actuation model as described in Grandia et al. [13]. The actuation model is detailed in Section VIII-G of the supplementary material. We assume that motors of the same model have nearly identical dynamics parameters due to manufacturing consistency. This assumption is empirically validated by performing sysID only five times—once for each Dynamixel motor model—and successfully transferring policies to a second ToddlerBot instance without additional sysID.

Teleoperation Device. Previous works [1, 48] demonstrate that teleoperation is one of the most effective ways to gather real-world data. Inspired by them, we develop a second upper body of ToddlerBot as the leader arms. Two force-sensitive resistors (FSRs) are embedded in the gripping area of the end effectors to detect compression force from the operator, allowing gripper movement based on force input.

We use a handheld gaming computer (either Steam Deck or ROG Ally X) to control the other body parts. The joysticks send velocity commands to walk, turn, and squat. Buttons trigger either programmed or trained policies, where holding a button executes the policy continuously, and releasing it stops the action. Buttons also provide direct control over neck and waist movements. The detailed mapping is described in Section VIII-H of the supplementary material.

IV. SYSTEM CONTROL

A. Keyframe Animation

Keyframe animation is a cornerstone of character animation, but it provides only kinematic data, with no guarantee of dynamic feasibility [21]. To address this, we developed software integrating MuJoCo [45] with a GUI, enabling real-time tuning and validation of keyframes and motion trajectories generated through linear interpolation with user-defined timings. With our high-fidelity digital twin, we efficiently generate open-loop trajectories such as cuddling, push-ups, and pull-ups that can be executed zero-shot in the real world.

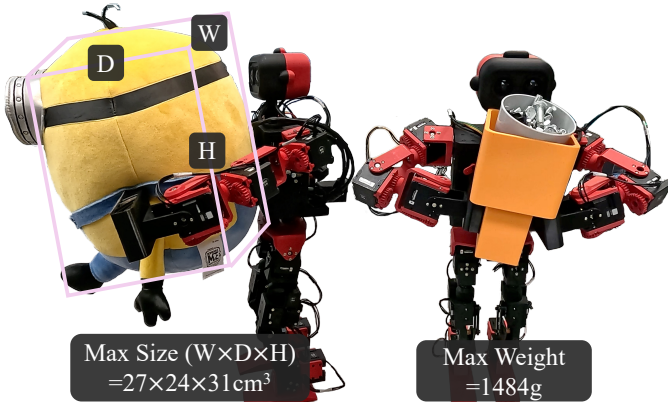


Figure 5: **Arm Span and Payload.** We show that with a torso dimension of $13 \times 9 \times 12 \text{ cm}^3$, ToddlerBot can grasp objects up to $27 \times 24 \times 31 \text{ cm}^3$, about 14 times the torso size. Additionally, ToddlerBot can lift weights up to 1484 g, which is 40% of its body weight (3484 g).

B. Reinforcement Learning

For walking and turning, we train a reinforcement learning (RL) policy, $\pi(\mathbf{a}_t | \mathbf{s}_t)$, which outputs \mathbf{a}_t as joint position setpoints for proportional-derivative (PD) controllers, based on the observable state \mathbf{s}_t :

$$\mathbf{s}_t = (\phi_t, \mathbf{c}_t, \Delta \mathbf{q}_t, \dot{\mathbf{q}}_t, \mathbf{a}_{t-1}, \boldsymbol{\theta}_t, \boldsymbol{\omega}_t), \quad (2)$$

where ϕ_t is a phase signal, \mathbf{c}_t represents velocity commands, $\Delta \mathbf{q}_t$ denotes the position offset relative to the neutral pose \mathbf{q}_0 , \mathbf{a}_{t-1} is the action from the previous time step, $\boldsymbol{\theta}_t$ represents the torso orientation, and $\boldsymbol{\omega}_t$ is the torso’s angular velocity. All inputs are normalized to ensure stable learning.

During PPO policy training [40], the environment generates the next state, \mathbf{s}_{t+1} , updates the phase signal, and returns a scalar reward $r_t = r(\mathbf{s}_t, \mathbf{a}_t, \mathbf{s}_{t+1}, \phi_t, \mathbf{c}_t)$. Following standard practice [13], the reward is decomposed as:

$$r_t = r_t^{\text{imitation}} + r_t^{\text{regularization}} + r_t^{\text{survival}}. \quad (3)$$

Among these components, $r_t^{\text{imitation}}$ encourages accurate imitation of the reference walking motion, which is generated using a closed-form ZMP (Zero Moment Point) solution [43]. $r_t^{\text{regularization}}$ incorporates heuristics of ideal walking motion, penalizes joint torques, and promotes smooth actions to minimize unnecessary movements. A survival reward r_t^{survival} prevents early episode termination during training. Additional details are provided in Section VIII-I of the supplementary material.

C. Imitation Learning

Real-world data collection involves a human operator guiding the leader’s arms to teleoperate the follower’s arms while using a joystick and buttons on a remote controller to control body movements.

During data collection, when the upper body tracks the position commands from the leader arms, ToddlerBot’s lower body employs a two-layer PD controller to maintain balance. The first layer is a Center of Mass (CoM) PD controller, which keeps the CoM close to the center of the support polygon. The

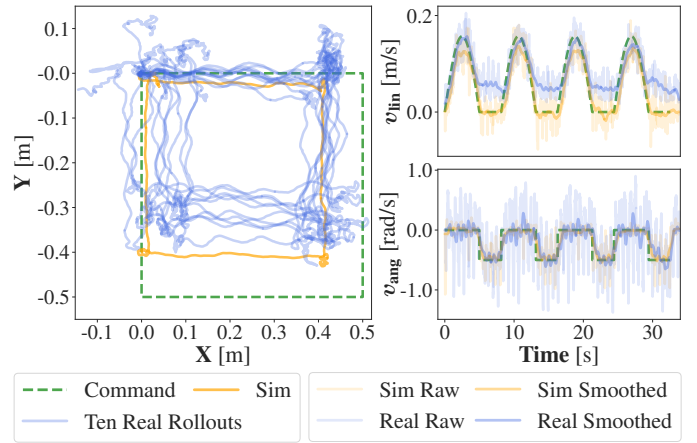


Figure 6: **Trajectory Tracking.** We present ten consecutive real-world rollouts of an RL walking policy tracking a square trajectory with a predefined velocity profile. Both raw and smoothed linear and angular velocity tracking are displayed, with real-world results averaged across trials.

Table II: Tracking Errors in Simulation versus the Real World

Tracking Errors	Simulation	Real-World
Position [m]	0.082	0.133 ± 0.018
Linear Velocity [m/s]	0.016	0.032 ± 0.002
Angular Velocity [rad/s]	0.056	0.113 ± 0.010

first layer addresses CoM shifts caused by arm movements, while the second layer manages lifting heavy objects. The second layer is a torso pitch PD controller, which uses IMU readings to ensure the torso remains upright.

With this setup, we can collect 60 trajectories in just 20 minutes for both bimanual and full-body manipulation tasks. The motor positions of the leader’s arms are recorded as the actions, while the motor positions of the follower robot, along with the RGB images captured from its camera, are recorded as observations. This data is subsequently used to train a diffusion policy [3], with further details provided in Section VIII-J of the supplementary material.

V. EXPERIMENTS

We conducted a series of experiments to show that ToddlerBot is capable, ML-compatible, and reproducible.

A. Capability: Arm Span, Payload, and Endurance

To evaluate ToddlerBot’s arm span and payload capacity, we teleoperate it to hug a test object using the compliant palm gripper while maintaining balance. In the arm span test, we show that with a torso dimension of $13 \times 9 \times 12 \text{ cm}^3$, ToddlerBot can grasp objects up to $27 \times 24 \times 31 \text{ cm}^3$, approximately 14 times its torso volume.

The payload test assesses both the upper body’s lifting capacity and the lower body’s ability to maintain balance. ToddlerBot successfully lifts up to 1484 g, 40% of its total weight (3484 g). To eliminate friction effects, we use a 3D-printed cup for the compliant palm gripper to lock in securely.

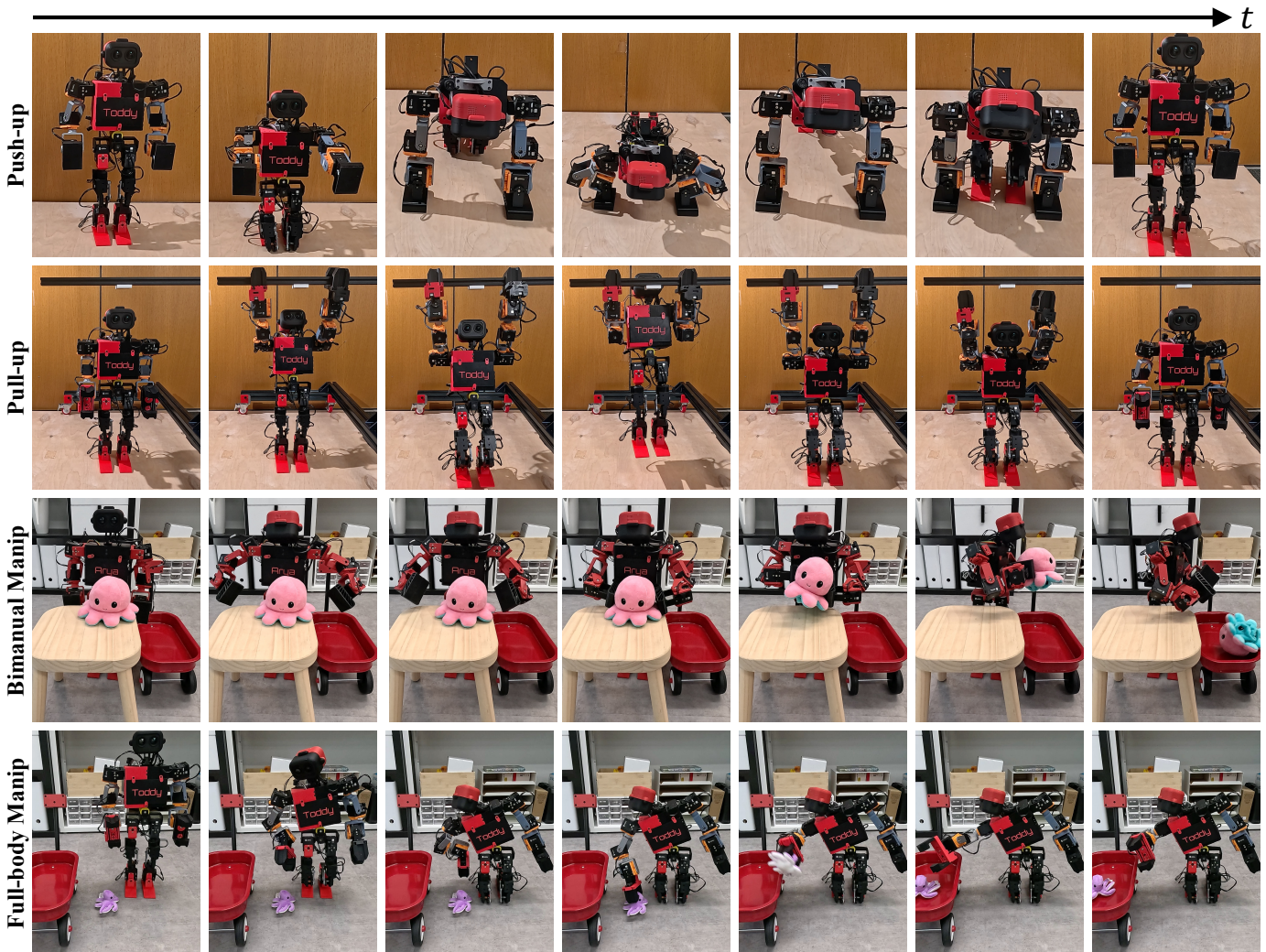


Figure 7: **Experiment Results.** We present a series of photos showcasing four different tasks: push-up, pull-up, bimanual, and full-body manipulation, demonstrating ToddlerBot’s capability in challenging locomotion and manipulation tasks.

To determine the true limit, we incrementally add screws to the cup until ToddlerBot falls over. Results are shown in Figure 5.

In the endurance test, ToddlerBot starts with a fully charged battery, running the walking RL policy while stepping in place. ToddlerBot achieved the longest streak of 19 minutes without falling. Over time, increased motor temperatures gradually pushed it outside the policy’s training distribution, leading to more frequent falls. ToddlerBot withstands up to 7 falls before breaking, but even then, repairs are quick—requiring only 21 minutes of 3D printing and 14 minutes of assembly, including removing the damaged part, installing the replacement, performing zero-point calibration, and rerunning the script.

B. Capability: Push-ups and Pull-ups

To demonstrate ToddlerBot’s ability to execute expressive and dynamic motions, we program push-ups and pull-ups in our keyframe software and perform a zero-shot sim-to-real transfer. For pull-ups, we use an AprilTag to help ToddlerBot accurately locate the horizontal bar. Both tasks require strong limbs, balanced upper-lower body strength, and precise

coordination, particularly when ToddlerBot transitions from a planking pose to standing after push-ups and when it releases the horizontal bar and lands after pull-ups. These open-loop transfers require only a single motion trajectory designed in simulation, highlighting the fidelity of our digital twin. Figure 7 showcases both tasks through a series of images.

C. ML-Compatibility: Omnidirectional Walking

To demonstrate ToddlerBot’s locomotion capabilities, we train RL walking policies to follow a square trajectory with a predefined velocity profile. Figure 6 and Table II present the results, with real-world tracking data collected via motion capture. Due to RL policy limitations, both simulation and real-world tracking deviate from the command, primarily because the learned walking policy struggles with in-place rotation, causing translation offsets. However, the sim-to-real gap is notably smaller than the tracking gap, supporting a successful zero-shot transfer. Additionally, we report a position tracking error variance of 0.018 m, linear velocity tracking

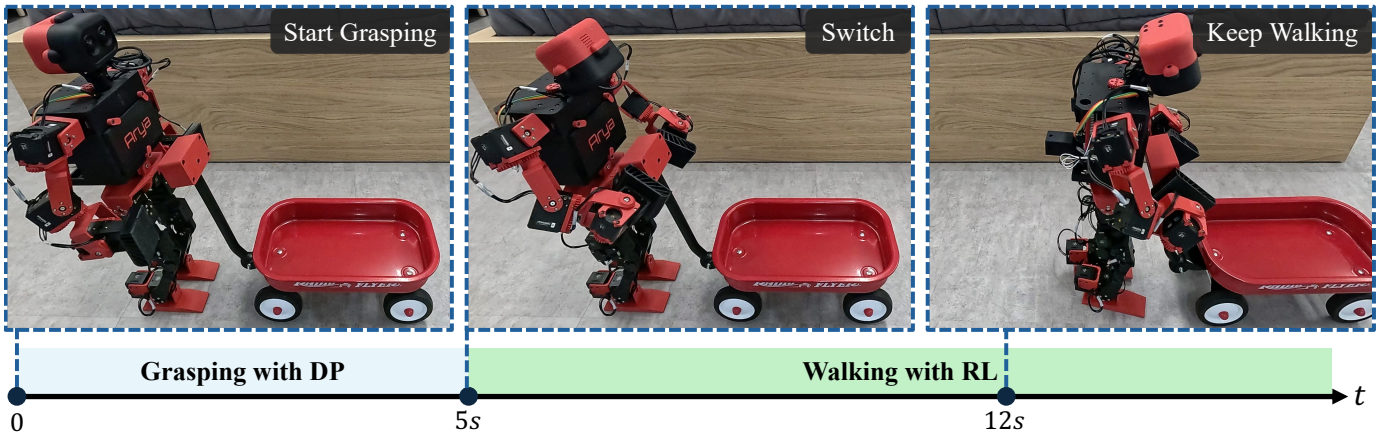


Figure 8: **Skill Chaining**. We demonstrate that ToddlerBot can seamlessly transition from a DP-based grasping skill to an RL-trained walking policy, enabling it to grasp the wagon handle and push it forward while maintaining its grip.

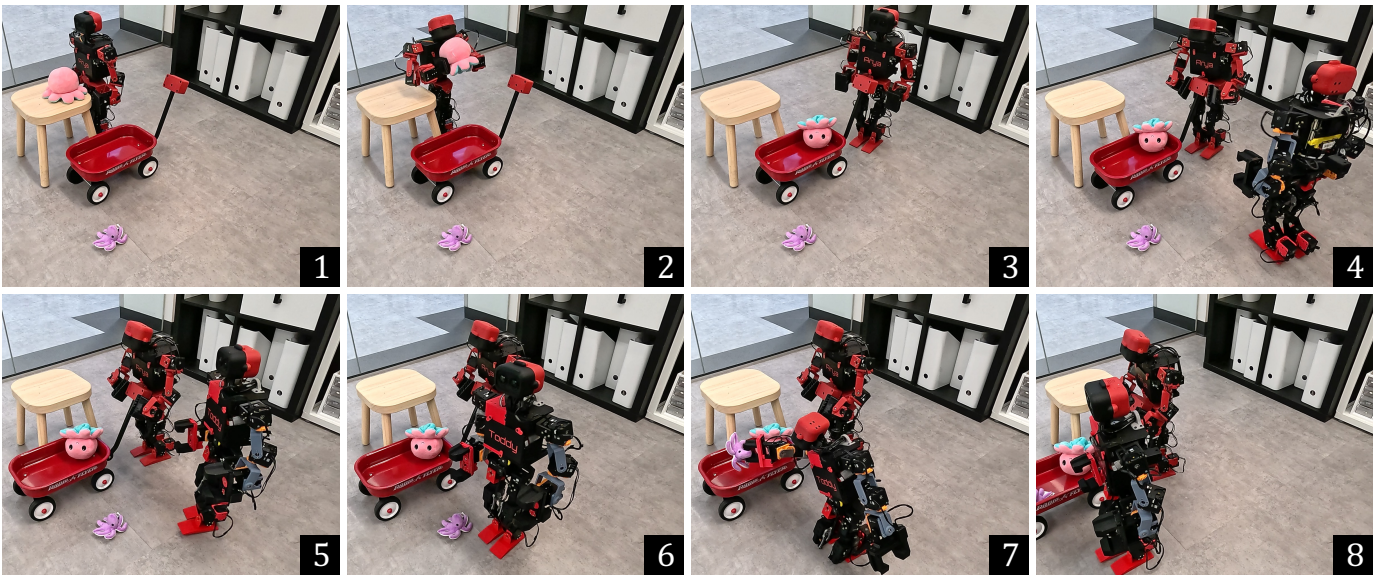


Figure 9: **Two-instance Collaboration**. In this task, two instances of ToddlerBot, Arya and Toddy, collaborate to clean up a toy session. (1) The scene begins with a pink octopus on the table, a purple octopus on the ground, a wagon, and Arya standing next to the table. (2) Arya picks up the pink octopus from the table and places it in the wagon. (3) Arya walks to the wagon handle. (4) Arya runs a grasping policy to grasp the wagon handle, while Toddy walks over. (5) Arya pushes the wagon toward the purple octopus and waits for Toddy. (6) Toddy reaches the pickup position. (7) Toddy kneels and picks up the purple octopus. (8) Finally, Arya and Toddy walk side by side, leaving the scene together.

error of 0.002 m/s, and angular velocity tracking error of 0.01 rad/s, which demonstrates good repeatability.

D. ML-Compatibility: Vision-based Manipulation

We show ToddlerBot’s ability to perform bimanual manipulation and full-body manipulation by transferring octopus toys from a table and the ground to a wagon. Both tasks are trained with RGB-based diffusion policy [3] with 60 demonstrations. Across 20 test trials, we achieve a 90% success rate for bimanual manipulation and 75% for full-body manipulation. We leverage a combination of open-loop motions and closed-loop policies to enhance data collection efficiency. In the bimanual task, the torso rotating and releasing motions are open-loop, while in full-body manipulation, kneeling down

is open-loop. The same motions are also used during policy evaluation. ToddlerBot’s onboard computing runs a 300M-parameter diffusion policy with about 100 ms latency, enabling real-time operation. Results are shown in Figure 7.

E. ML-Compatibility: Skill Chaining

To test the system’s ability to combine locomotion and manipulation skills, we test the wagon-pushing task (Figure 8), which requires the robot to first perform vision-based grasping and then walk forward. To do so, ToddlerBot first executes a diffusion policy to grasp the handle, while maintaining that pose, switched to the RL policy to push the wagon forward. To enable ToddlerBot to walk while maintaining its grip, we sample the end pose of the upper body from the grasping

policy’s training data (60 demonstrations) during RL training.

F. Reproducibility: Hardware and Policies

To demonstrate hardware reproducibility, we recruit a CS-major student with no prior hardware experience to assemble a second ToddlerBot using our manuals as shown in Figure 15 of the supplementary material and our open-source assembly videos. The student independently completes the assembly in three days, including the time required for 3D printing.

For policy reproducibility, we run the manipulation policy trained on data collected with one instance on the other instance, achieving the same success rate of 90% across 20 trials. We also successfully transfer the RL walking policy between both robots. To further showcase the equivalent performance of both ToddlerBot instances, we have them collaborate on a long-horizon room tidying task, as shown in Figure 9.

VI. LIMITATIONS AND FUTURE WORK

ToddlerBot’s performance in more agile tasks is constrained by the off-the-shelf motors’ max speed, max torque, and communication speed. Rather than achieving superhuman capabilities, ToddlerBot aligns more closely with average human performance in loco-manipulation tasks. Additionally, its scale limits interaction with human-sized objects, though this does not hinder research if appropriately sized objects are used.

To overcome these limitations, we are developing customized communication boards and improving motor system identification to maximize performance. We also aim to improve sensing capabilities, including stereo vision for depth perception, additional IMUs for improved state estimation, and tactile sensors for richer feedback.

VII. CONCLUSIONS

In conclusion, we demonstrate that ToddlerBot is ML-compatible, capable, and reproducible through a series of tests and loco-manipulation tasks. While humanoid research is often associated with locomotion, ToddlerBot extends beyond this to support full-body manipulation, character animation, human-robot interaction, and various ML applications, making it a versatile research platform. With ToddlerBot fully open-source, we hope to empower researchers to explore new directions in humanoid research and encourage open collaboration in the community.

ACKNOWLEDGMENTS

The authors would like to express their gratitude to Kaizhe Hu for assembling the second instance of ToddlerBot and assisting with keyframe animation and demo recording. We also extend our thanks to Huy Ha, Yen-Jen Wang, Pei Xu, and Yifan Hou for their insightful discussions on locomotion, and to Sirui Chen, Chen Wang, and Yunfan Jiang for valuable input on manipulation policy deployment. We are grateful to Albert Wu for his guidance on mathematical formulation and notation. Additionally, we thank João Pedro Araújo for his assistance with the motion capture system. Finally, we appreciate the helpful discussions from all members of

TML and REALab. This work was supported by National Science Foundation NSF-FRR-2153854, NSF-2143601, NSF-2037101, Sloan Fellowship, Stanford Institute for Human-Centered Artificial Intelligence, and Stanford Wu Tsai Human Performance Alliance.

REFERENCES

- [1] Jorge Aldaco, Travis Armstrong, Robert Baruch, Jeff Bingham, Sanky Chan, Debidatta Dwibedi, Chelsea Finn, Pete Florence, Spencer Goodrich, Wayne Gramlich, Alexander Herzog, Jonathan Hoeh, Thinh Nguyen, Ian Storz, Baruch Tabanpour, Jonathan Tompson, Ayzaan Wahid, Ted Wahrburg, Sichun Xu, Sergey Yaroshenko, and Tony Z Zhao. [ALOHA 2: An Enhanced Low-Cost Hardware for Bimanual Teleoperation](#), 2024.
- [2] Raunaq Bhirangi, Abigail DeFranco, Jacob Adkins, Carmel Majidi, Abhinav Gupta, Tess Hellebrekers, and Vikash Kumar. [All the Feels: A Dexterous Hand With Large-Area Tactile Sensing](#). *IEEE Robotics and Automation Letters*, 8(12):8311–8318, December 2023. ISSN 2377-3766. doi: 10.1109/LRA.2023.3327619.
- [3] Cheng Chi, Siyuan Feng, Yilun Du, Zhenjia Xu, Eric Cousineau, Benjamin Burchfiel, and Shuran Song. [Diffusion Policy: Visuomotor Policy Learning via Action Diffusion](#). In *Robotics: Science and Systems XIX*. Robotics: Science and Systems Foundation, July 2023. ISBN 978-0-9923747-9-2. doi: 10.15607/RSS.2023.XIX.026.
- [4] Cheng Chi, Zhenjia Xu, Chuer Pan, Eric Cousineau, Benjamin Burchfiel, Siyuan Feng, Russ Tedrake, and Shuran Song. [Universal Manipulation Interface: In-The-Wild Robot Teaching Without In-The-Wild Robots](#). In *Robotics: Science and Systems XX*. Robotics: Science and Systems Foundation, July 2024. ISBN 9798990284807. doi: 10.15607/RSS.2024.XX.045.
- [5] Matthew Chignoli, Donghyun Kim, Elijah Stanger-Jones, and Sangbae Kim. [The MIT Humanoid Robot: Design, Motion Planning, and Control For Acrobatic Behaviors](#). In *2020 IEEE-RAS 20th International Conference on Humanoid Robots (Humanoids)*, pages 1–8, Munich, Germany, July 2021. IEEE. ISBN 978-1-72819-372-4. doi: 10.1109/HUMANOIDS47582.2021.9555782.
- [6] Open X-Embodiment Collaboratoin. [Open X-Embodiment: Robotic Learning Datasets and RT-X Models : Open X-Embodiment Collaboration0](#). In *2024 IEEE International Conference on Robotics and Automation (ICRA)*, pages 6892–6903, May 2024. doi: 10.1109/ICRA57147.2024.10611477.
- [7] Jia Deng, Wei Dong, Richard Socher, Li-Jia Li, Kai Li, and Li Fei-Fei. [ImageNet: A Large-Scale Hierarchical Image Database](#). In *2009 IEEE Conference on Computer Vision and Pattern Recognition*, pages 248–255, June 2009. doi: 10.1109/CVPR.2009.5206848.
- [8] Boston Dynamics. [Atlas](#), 2024.
- [9] FigureAI. [Figure](#), 2024.
- [10] FOURIER-Robotics. [FOURIER-Robotics](#), 2024.
- [11] C. Daniel Freeman, Erik Frey, Anton Raichuk, Sertan

- Girgin, Igor Mordatch, and Olivier Bachem. [Brax - A Differentiable Physics Engine for Large Scale Rigid Body Simulation](#), 2021.
- [12] Zipeng Fu, Qingqing Zhao, Qi Wu, Gordon Wetzstein, and Chelsea Finn. [HumanPlus: Humanoid Shadowing and Imitation from Humans](#). In *8th Annual Conference on Robot Learning*, September 2024.
- [13] Ruben Grandia, Espen Knoop, Michael Hopkins, Georg Wiedebach, Jared Bishop, Steven Pickles, David Müller, and Moritz Bächer. [Design and Control of a Bipedal Robotic Character](#). In *Robotics: Science and Systems XX*. Robotics: Science and Systems Foundation, July 2024. ISBN 9798990284807. doi: 10.15607/RSS.2024.XX.103.
- [14] Martin Grimmer, Ahmed A. Elshamanhory, and Philipp Beckerle. [Human Lower Limb Joint Biomechanics in Daily Life Activities: A Literature Based Requirement Analysis for Anthropomorphic Robot Design](#). *Frontiers in Robotics and AI*, 7, February 2020. ISSN 2296-9144. doi: 10.3389/frobt.2020.00013.
- [15] Xinyang Gu, Yen-Jen Wang, and Jianyu Chen. [Humanoid-Gym: Reinforcement Learning for Humanoid Robot with Zero-Shot Sim2Real Transfer](#), April 2024.
- [16] Xinyang Gu, Yen-Jen Wang, Xiang Zhu, Chengming Shi, Yanjiang Guo, Yichen Liu, and Jianyu Chen. [Advancing Humanoid Locomotion: Mastering Challenging Terrains with Denoising World Model Learning](#). In *Robotics: Science and Systems*, 2024.
- [17] Tuomas Haarnoja, Ben Moran, Guy Lever, Sandy H. Huang, Dhruva Tirumala, Jan Humplik, Markus Wulfmeier, Saran Tunyasuvunakool, Noah Y. Siegel, Roland Hafner, Michael Bloesch, Kristian Hartikainen, Arunkumar Byravan, Leonard Hasenclever, Yuval Tassa, Fereshteh Sadeghi, Nathan Batchelor, Federico Casarini, Stefano Saliceti, Charles Game, Neil Sreendra, Kushal Patel, Marlon Gwira, Andrea Huber, Nicole Hurley, Francesco Nori, Raia Hadsell, and Nicolas Heess. [Learning Agile Soccer Skills for a Bipedal Robot with Deep Reinforcement Learning](#). *Science Robotics*, 9(89): eadi8022, April 2024. doi: 10.1126/scirobotics.adi8022.
- [18] Kaiming He, Xiangyu Zhang, Shaoqing Ren, and Jian Sun. [Deep Residual Learning for Image Recognition](#). In *2016 IEEE Conference on Computer Vision and Pattern Recognition (CVPR)*, pages 770–778, Las Vegas, NV, USA, June 2016. IEEE. ISBN 978-1-4673-8851-1. doi: 10.1109/CVPR.2016.90.
- [19] Tairan He, Zhengyi Luo, Xialin He, Wenli Xiao, Chong Zhang, Weinan Zhang, Kris M. Kitani, Changliu Liu, and Guanya Shi. [OmniH2O: Universal and Dexterous Human-to-Humanoid Whole-Body Teleoperation and Learning](#). In *2nd Workshop on Dexterous Manipulation: Design, Perception and Control (RSS)*, July 2024.
- [20] Tairan He, Wenli Xiao, Toru Lin, Zhengyi Luo, Zhenjia Xu, Zhenyu Jiang, Jan Kautz, Changliu Liu, Guanya Shi, Xiaolong Wang, Linxi Fan, and Yuke Zhu. [HOVER: Versatile Neural Whole-Body Controller for Humanoid Robots](#), October 2024.
- [21] M. Izani, Aishah, A.R. Eshaq, and Norzaiha. [Keyframe Animation and Motion Capture for Creating Animation: A Survey and Perception from Industry People](#). In *Proceedings. Student Conference on Research and Development, 2003. SCORED 2003.*, pages 154–159, August 2003. doi: 10.1109/SCORED.2003.1459684.
- [22] Mazeyu Ji, Xuanbin Peng, Fangchen Liu, Jialong Li, Ge Yang, Xuxin Cheng, and Xiaolong Wang. [ExBody2: Advanced Expressive Humanoid Whole-Body Control](#), December 2024.
- [23] Benjamin Katz, Jared Di Carlo, and Sangbae Kim. [Mini Cheetah: A Platform for Pushing the Limits of Dynamic Quadruped Control](#). In *2019 International Conference on Robotics and Automation (ICRA)*, pages 6295–6301, May 2019. doi: 10.1109/ICRA.2019.8793865.
- [24] Nathan Kau. [Stanford Pupper: A Low-Cost Agile Quadruped Robot for Benchmarking and Education](#), February 2022.
- [25] Alexander Khazatsky, Karl Pertsch, Suraj Nair, Ashwin Balakrishna, Sudeep Dasari, Siddharth Karamcheti, Soroush Nasiriany, Mohan Srirama, Lawrence Chen, Kirsty Ellis, Peter Fagan, Joey Hejna, Masha Itkina, Marion Lepert, Yecheng Ma, Patrick Miller, Jimmy Wu, Suneel Belkhale, Shivin Dass, Huy Ha, Arhan Jain, Abraham Lee, Youngwoon Lee, Marius Memmel, Sungjae Park, Ilija Radosavovic, Kaiyuan Wang, Albert Zhan, Kevin Black, Cheng Chi, Kyle Hatch, Shan Lin, Jingpei Lu, Jean Mercat, Abdul Rehman, Pannag Sanketi, Archit Sharma, Cody Simpson, Quan Vuong, Homer Walke, Blake Wulfe, Ted Xiao, Jonathan Yang, Arefeh Yavary, Tony Zhao, Christopher Agia, Rohan Bajjal, Mateo Castro, Daphne Chen, Qiuyu Chen, Trinity Chung, Jaimyn Drake, Ethan Foster, Jensen Gao, David Herrera, Minho Heo, Kyle Hsu, Jiaheng Hu, Donovan Jackson, Charlotte Le, Yunshuang Li, Roy Lin, Zehan Ma, Abhiram Maddukuri, Suvir Mirchandani, Daniel Morton, Tony Nguyen, Abigail O’Neill, Rosario Scalise, Derick Seale, Victor Son, Stephen Tian, Emi Tran, Andrew Wang, Yilin Wu, Annie Xie, Jingyun Yang, Patrick Yin, Yunchu Zhang, Osbert Bastani, Glen Berseth, Jeannette Bohg, Ken Goldberg, Abhinav Gupta, Abhishek Gupta, Dinesh Jayaraman, Joseph Lim, Jitendra Malik, Roberto Martín-Martín, Subramanian Ramamoorthy, Dorsa Sadigh, Shuran Song, Jiajun Wu, Michael Yip, Yuke Zhu, Thomas Kollar, Sergey Levine, and Chelsea Finn. [DROID: A Large-Scale In-The-Wild Robot Manipulation Dataset](#). In *Robotics: Science and Systems XX*. Robotics: Science and Systems Foundation, July 2024. ISBN 9798990284807. doi: 10.15607/RSS.2024.XX.120.
- [26] Joonho Lee, Jemin Hwangbo, Lorenz Wellhausen, Vladlen Koltun, and Marco Hutter. [Learning Quadrupedal Locomotion over Challenging Terrain](#). *Science Robotics*, 5(47):eabc5986, October 2020. doi: 10.1126/scirobotics.abc5986.
- [27] Qiayuan Liao, Bike Zhang, Xuanyu Huang, Xiaoyu

- Huang, Zhongyu Li, and Koushil Sreenath. [Berkeley Humanoid: A Research Platform for Learning-based Control](#), July 2024.
- [28] Yeting Liu, Junjie Shen, Jingwen Zhang, Xiaoguang Zhang, Taoyuanmin Zhu, and Dennis Hong. [Design and Control of a Miniature Bipedal Robot with Proprioceptive Actuation for Dynamic Behaviors](#). In *2022 International Conference on Robotics and Automation (ICRA)*, pages 8547–8553, Philadelphia, PA, USA, May 2022. IEEE. ISBN 978-1-72819-681-7. doi: 10.1109/ICRA46639.2022.9811790.
- [29] Chenhao Lu, Xuxin Cheng, Jialong Li, Shiqi Yang, Mazeyu Ji, Chengjing Yuan, Ge Yang, Sha Yi, and Xiaolong Wang. [Mobile-TeleVision: Predictive Motion Priors for Humanoid Whole-Body Control](#), December 2024.
- [30] Ajay Mandlekar, Jonathan Booher, Max Spero, Albert Tung, Anchit Gupta, Yuke Zhu, Animesh Garg, Silvio Savarese, and Li Fei-Fei. [Scaling Robot Supervision to Hundreds of Hours with RoboTurk: Robotic Manipulation Dataset through Human Reasoning and Dexterity](#). In *2019 IEEE/RSJ International Conference on Intelligent Robots and Systems (IROS)*, pages 1048–1055, November 2019. doi: 10.1109/IROS40897.2019.8968114.
- [31] NAO H25. [NAO H25 — Aldebaran 2.1.4.13 Documentation](#), 2018.
- [32] Alberto Parmiggiani, Marco Maggiali, Lorenzo Natale, Francesco Nori, Alexander Schmitz, Nikos Tsagarakis, José Santos Victor, Francesco Becchi, Giulio Sandini, and Giorgio Metta. [THE DESIGN OF THE iCub HUMANOID ROBOT](#). *International Journal of Humanoid Robotics*, 09(04):1250027, December 2012. ISSN 0219-8436. doi: 10.1142/S0219843612500272.
- [33] Agility Robotics. [Cassie Sets a Guinness World Record](#), 2016.
- [34] Agility Robotics. [Agility Robotics](#), 2024.
- [35] Booster Robotics. [Booster](#), 2024.
- [36] ROBOTIS. [OP3 E-Manual](#), 2018.
- [37] ROBOTIS. [Dynamixel-X E-Manual](#), 2018.
- [38] Branden Romero, Hao-Shu Fang, Pulkit Agrawal, and Edward Adelson. [EyeSight Hand: Design of a Fully-Actuated Dexterous Robot Hand with Integrated Vision-Based Tactile Sensors and Compliant Actuation](#), August 2024.
- [39] Nikita Rudin, David Hoeller, Philipp Reist, and Marco Hutter. [Learning to Walk in Minutes Using Massively Parallel Deep Reinforcement Learning](#). In *Proceedings of the 5th Conference on Robot Learning*, pages 91–100. PMLR, January 2022.
- [40] John Schulman, Filip Wolski, Prafulla Dhariwal, Alec Radford, and Oleg Klimov. [Proximal Policy Optimization Algorithms](#). *ArXiv*, July 2017.
- [41] Kenneth Shaw, Ananye Agarwal, and Deepak Pathak. [LEAP Hand: Low-Cost, Efficient, and Anthropomorphic Hand for Robot Learning](#). In *Robotics: Science and Systems XIX*. Robotics: Science and Systems Foundation, July 2023. ISBN 978-0-9923747-9-2. doi: 10.15607/RSS.2023.XIX.089.
- [42] Jie Tan, Tingnan Zhang, Erwin Coumans, Atil Iscen, Yunfei Bai, Danijar Hafner, Steven Bohez, and Vincent Vanhoucke. [Sim-to-Real: Learning Agile Locomotion For Quadruped Robots](#). In *Robotics: Science and Systems XIV*. Robotics: Science and Systems Foundation, June 2018. ISBN 978-0-9923747-4-7. doi: 10.15607/RSS.2018.XIV.010.
- [43] Russ Tedrake, Scott Kuindersma, Robin Deits, and Kanako Miura. [A Closed-Form Solution for Real-Time ZMP Gait Generation and Feedback Stabilization](#). In *2015 IEEE-RAS 15th International Conference on Humanoid Robots (Humanoids)*, pages 936–940, Seoul, South Korea, November 2015. IEEE. ISBN 978-1-4799-6885-5. doi: 10.1109/HUMANOIDS.2015.7363473.
- [44] Tesla. [AI & Robotics](#), 2024.
- [45] Emanuel Todorov, Tom Erez, and Yuval Tassa. [MuJoCo: A Physics Engine for Model-Based Control](#). In *2012 IEEE/RSJ International Conference on Intelligent Robots and Systems*, pages 5026–5033, October 2012. doi: 10.1109/IROS.2012.6386109.
- [46] Unitree. [Unitree H1 - Unitree’s First Universal Humanoid Robot - Unitree](#), 2024.
- [47] Unitree. [Unitree G1 - Humanoid Agent AI Avatar - Unitree](#), 2024.
- [48] Philipp Wu, Fred Shentu, Xingyu Lin, and Pieter Abbeel. [GELLO: A General, Low-Cost, and Intuitive Teleoperation Framework for Robot Manipulators](#). In *Towards Generalist Robots: Learning Paradigms for Scalable Skill Acquisition @ CoRL2023*, October 2023.
- [49] Boxi Xia, Bokuan Li, Jacob Lee, Michael Scutari, and Boyuan Chen. [The Duke Humanoid: Design and Control For Energy Efficient Bipedal Locomotion Using Passive Dynamics](#), September 2024.
- [50] Tony Zhao, Vikash Kumar, Sergey Levine, and Chelsea Finn. [Learning Fine-Grained Bimanual Manipulation with Low-Cost Hardware](#). In *Robotics: Science and Systems XIX*. Robotics: Science and Systems Foundation, July 2023. ISBN 978-0-9923747-9-2. doi: 10.15607/RSS.2023.XIX.016.

VIII. SUPPLEMENTARY MATERIALS

A. Ease of Assembly and Maintenance

The ease of assembly and maintenance is crucial yet difficult to specify, as it requires mentally simulating the assembly and disassembly process. In early iterations, we explicitly selected screw types and ensured unobstructed tool access, which allowed a clear assembly direction for the screwdriver. We also prioritized modular design, allowing individual parts to be removed independently. These considerations significantly improve maintainability and simplify repairs.

B. Power Factor

When comparing the performance of humanoids with different scales and weights, it is essential to establish a meaningful metric. Directly having a full-sized 180 cm humanoid and a 50 cm scaled humanoid both jump 50 cm or run at 3 m/s is not a fair comparison. A more reasonable approach is to normalize performance metrics, for example by evaluating a jump at 10% of body height or a running speed of twice the body length per second. Formally, we say two humanoid having the **same performance** if they execute the same sequence of joint motions over a time span T , and their total power consumption is the same fraction of their motors' maximum power:

$$\frac{\int_0^T p(t)dt}{\sum_{i=0}^N |\tau_i^{\max} \dot{q}_i|} \approx \frac{\Delta h \cdot mg}{\sum_{i=0}^N |\tau_i^{\max} \dot{q}_i|} \approx \frac{h \cdot mg}{\sum_{i=0}^N |\tau_i^{\max} \dot{q}_i|}, \quad (4)$$

where $p(t)$ is the humanoid's power output at time t . τ_i^{\max} and \dot{q}_i are the maximum torque and joint velocity of the i -th motor in the humanoid respectively. Moreover, when computing the maximum power, we take the absolute value to ensure all motors perform positive work. For the numerator, the integral of the power output over T , which is equivalent to the work done by the robot, can be approximated by the gravitational energy gained: $\Delta h \cdot mg$. Since Δh is approximately proportional to the height of the humanoid, we further replace Δh with just the humanoid's height h .

Based on Equation 4, we now define a metric, power factor, to measure the performance of a humanoid:

$$\tilde{p} = \frac{\sum_{i=0}^N |\tau_i^{\max}|}{h \cdot mg}. \quad (5)$$

Note that we flip the fraction from Equation 4 to make the power factor value increase as the utilized torque ratio decreases. We also drop \dot{q} as the same sequence of joint motion would be executed when using power factor to compare the performance of humanoids.

In summary, our proposed \tilde{p} naturally incorporates the crucial physical parameters: height, mass, and gravity, to give a fair measure of motion capability across humanoids of very different scales. Achieving or surpassing the human threshold \tilde{p} is indicative of human-like dynamic potential, although practical constraints (e.g., battery efficiency, control complexity, safety) may set an upper bound on how large \tilde{p} should be in a real-world humanoid design.

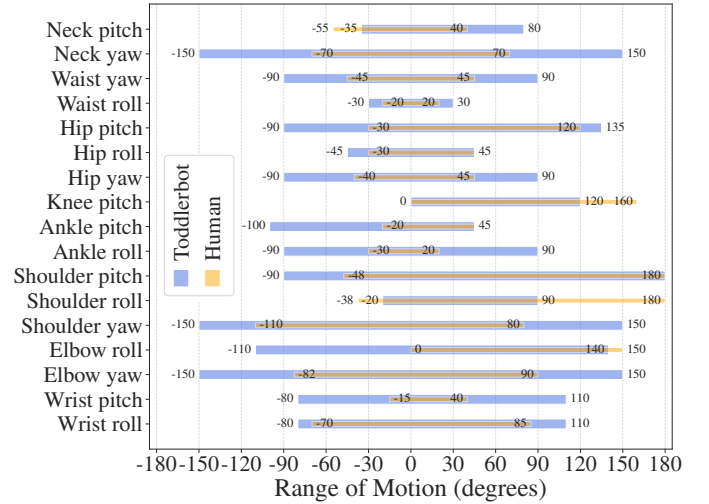


Figure 10: **Range of Motion.** We show that ToddlerBot has near-human or even superhuman mobility in most joints. Negative values represent extensions, adductions, and inversions, while flexions, abductions, and eversions are positive.

C. Range of Motion

We design each joint's range of motion based on human biomechanics, optimizing geometries to prevent self-collisions and achieve near-human or even superhuman mobility in most joints (Figure 10). The additional extension of the ankle pitch partially compensates for the 40° gap in knee pitch and the absence of toes. For shoulder roll, although 90° is limited compared to a human's shoulder abduction, the same hand-up pose can be achieved by actuating the shoulder pitch joint.

D. Transmission Mechanisms

Placing motors directly at the joint is often impractical. With carefully designed transmission mechanisms, motors can be relocated outside the interference zone, amplify torque output, and offload mechanical stress to the structure. This section highlights key design features, including spur gears, coupled bevel gears, and parallel linkages, as shown in Figure 11.

Each transmission type offers unique benefits. To start with, spur gears provide three advantages:

- 1) **Relocated joint axis:** A 1:1 spur gear set allows repositioning of the joint axis to a more convenient in-plane location without affecting the motor's range of motion. This is widely used in ToddlerBot's arm.
- 2) **Torque modification:** A ratioed spur gear set adjusts the final torque output, which is particularly useful for the parallel jaw gripper.
- 3) **Load distribution:** When a motor's output shaft has significant free play, as in Dynamixel XC330, where it is supported only by a Teflon bushing, using it directly as the joint axis is undesirable. A 1:1 spur gear set enables a reinforced secondary axis with planar bearings and metal shafts to carry the load, protecting the motor from transverse forces. This approach is used in the hip yaw joints, where torque demands are low, but load-bearing capacity is critical.

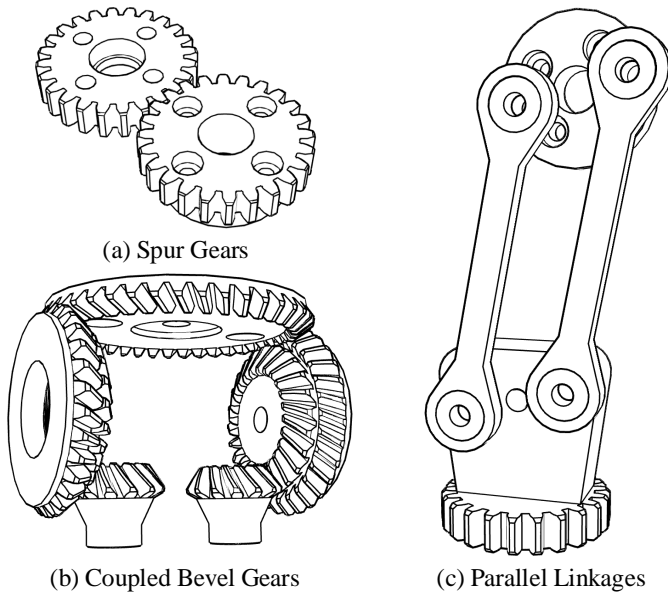


Figure 11: **Transmission Mechanisms.** We show three design primitives in ToddlerBot’s mechanical design: spur gears, coupled bevel gears, and parallel linkages.

Table III: Dynamixel Motor Assignments for ToddlerBot.

Motor Model	Stall Torque ^(a)	Assigned DoFs
XC330-T288	1.0	Neck PY ^(b) , Waist RY, Hip Y, Gripper
XC430-T240BB	1.9	Shoulder P, Ankle R
XM430-W210	3.0	Knee P, Ankle P
2XL430-W250	1.5	Shoulder RY, Elbow RY, Wrist RP
2XC430-W250	1.8	Hip RP

^(a) The Stall Torque data are measured at 12V as reported on the Dynamixel official website [37]. The unit is Nm.

^(b) R, P, and Y denote roll, pitch, and yaw respectively.

With precise tolerance tuning, 3D-printed bevel gears provide a highly interlocking design with minimal backlash, while still being structurally strong. They also offer three key advantages:

- 1) **Rotated joint axis:** A coupled bevel gear set enables a parallel waist mechanism, where two motors in the same orientation drive two perpendicular DoFs.
- 2) **Combined torque output:** On each axis, both motors contribute to the driving torque, enhancing power and efficiency. This is critical, as a single Dynamixel XC330 lacks the power to drive the entire upper body, but two motors combined are sufficient.
- 3) **Compact actuation:** In the waist, where space is highly constrained, a coupled bevel gear set allows the compact integration of two DoFs.

Lastly, parallel linkages allow the motor to be positioned away from the joint axis, as seen in the knee and neck pitch. Despite a limited range of motion (usually $< 160^\circ$), this design is easy to assemble and efficiently transfers high torque when paired with ball bearings. They provide three key benefits:

- 1) **Compact design:** This enables a cleaner, more compact neck design by placing the motor inside the head.

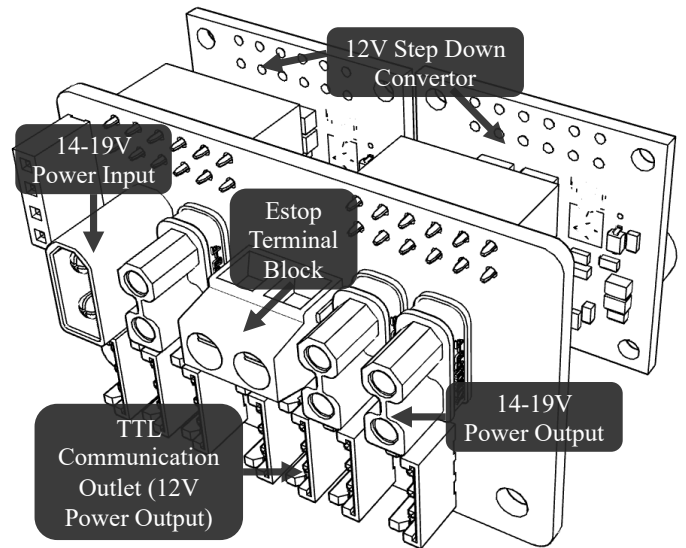


Figure 12: **Power Distribution.** We show the power distribution board design, including four XT30 power plugs, an Estop terminal block, seven JST EH TTL communication outlets, and two 12V step-down converters.

- 2) **Reduced Inertia:** The knee motor is placed higher to reduce rotational inertia.
- 3) **Structural Efficiency:** In the thigh, the knee motor is bolted to a 3D-printed structure for better load distribution, increased rigidity, and reduced weight.

A potential drawback of these transmission mechanisms is their inaccurate simulation modeling. However, in MuJoCo [45], we mitigate this by using joint equality constraints for spur gears, fixed tendons for coupled bevel gears, and weld constraints for parallel linkages. This approach has empirically shown a small sim2real gap, as demonstrated in Section V.

E. Motor Selection

Given ToddlerBot’s size constraint and 30-DoF design, Brushless Direct Drive (BLDC) motors are not a viable option. As BLDC motors shrink, their winding thickness decreases, reducing current capacity and torque constant. Despite their high power density, they still require a high-ratio gearbox, making them less suitable given our limited space budget. We initially explored electric linear actuators but found them unsuitable due to insufficient power density and low control frequency. After a few iterations, we narrowed our choices to servo motors, ultimately selecting Dynamixel motors for their desirable performance and well-documented support. Given that reproducibility is a hard constraint in our system, we believe a pure-Dynamixel design is the most feasible to reproduce, especially for those with limited hardware experience.

For the Dynamixel motors, the smallest units start at approximately 50 g. This allows us to estimate the total weight as $3100 = 30 \times 50$ (motors) + 600 (computer, battery, camera) + 1000 (3D-printed structure and metal hardware) g.

To estimate the torque required for each joint to achieve human-like motions, we followed the reference values from

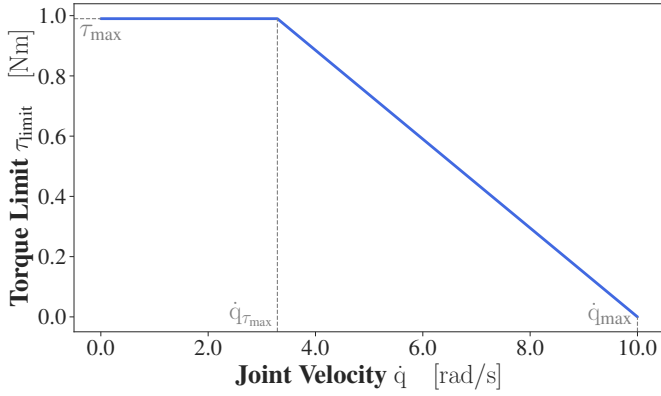


Figure 13: The sysIDed relationship between torque limit τ_{limit} and joint velocity \dot{q} for Dynamixel XC330.

Table IV: SysIDed Parameters for Dynamixel Motors.

Parameter	2XL430	XC330	XC430	2XC430	XM430
Damping ^(a)	0.12	0.134	0.127	0.075	0.08
Armature	0.0042	0.0035	0.004	0.0044	0.0012
Friction Loss	0.292	0.014	0.069	0.252	0.134
τ_{max}	1.55	0.99	1.45	1.74	1.86
$\dot{q}_{\tau_{\text{max}}}$	3.24	3.29	4.99	2.84	4.22
\dot{q}_{max}	19.91	10.0	10.0	10.0	10.0

^(a) The unit of damping is Nms/rad, the unit of armature is kgm², the unit of τ_{max} is Nm, and the unit of $\dot{q}_{\tau_{\text{max}}}$ and \dot{q}_{max} is rad/s.

[14] and Equation 1 to derive the torque estimation:

$$\tau_{\text{robot}} = \frac{h_{\text{robot}} \cdot m_{\text{robot}}}{h_{\text{human}} \cdot m_{\text{human}}} \cdot \tau_{\text{human}}. \quad (6)$$

With an estimated height of 0.5 m and weight of 3.1 kg, the required lower limb torque for ToddlerBot to perform the most demanding tasks—assuming an optimal control policy—such as running and slope climbing [14], is estimated as follows: $\tau_{\text{robot}}^{\text{knee}} = 2.35$ Nm, $\tau_{\text{robot}}^{\text{ankle pitch}} = 2.66$ Nm, $\tau_{\text{robot}}^{\text{hip pitch}} = 1.77$ Nm.

As shown in Table III, XM430 is the only option that provides sufficient torque for the knee and ankle pitch joints. Its metal gears, low backdrive resistance, and high torque output make it ideal for these joints which directly impact walking stability. For the hip, we use 2XC430s for roll and pitch, as they provide sufficient torque while maintaining a compact design, integrating two actuated DoFs in a single housing. This setup allows for a greater range of motion compared to placing two XC430s sequentially. The XC330 series is the smallest and most cost-effective in the lineup but has higher tracking errors and backlash. Therefore, we use XC330s on joints with lower torque demands or strict weight and space constraints, such as the neck, waist, hip yaw, and parallel jaw gripper. 2XL430, a lower-cost variant of the 2XC430, is used in the arm to balance performance and cost, ensuring minimal performance loss while maximizing affordability. For the remaining joints, including shoulder pitch and ankle roll, XC430 is used as a standard choice.

F. Power

With the motor selection finalized, we can estimate the power budget. The computer and camera together consume approximately 15 W under typical operating conditions. Actual walking power consumption depends on the energy efficiency of the control policy, but preliminary analysis suggests that the upper body requires minimal power during walking, as it carries no additional load. The lower body operates with alternating support, meaning only one leg is actively working at a time. Assuming a 70% duty cycle, total motor power consumption is estimated at 60 W, requiring a 75 Wh battery for one hour of continuous walking.

For the battery, we offer two options: A 2000 mAh LiPo battery (215 g) available off-the-shelf or a custom-made 4-cell 21700 battery with 5000 mAh, which has higher energy density and weighs 330 g. In practice, the battery lasts 3–5 hours in research settings where the robot walks intermittently. The peak power output from the battery is $14.8 \text{ V} \times 25 \text{ A} = 370 \text{ W}$, sufficient to power all the joints. When debugging without a battery, a 15 V 300 W power supply is a practical alternative—safer and easier to obtain than those required for full-scale humanoids, which often exceed 2 kW and 60 V.

As shown in Figure 12, the battery provides a 14 – 19V input, regulated to 12V via dual step-down converters to power the motors through TTL communication outlets. An E-stop terminal block controls motor power, enabling emergency reboots. The 14 – 19V output powers the Jetson Orin NX, which remains on when the battery is connected to prevent data loss from an abrupt shutdown.

G. Actuation Model

Inspired by Grandia et al. [13], we design our actuation model as follows. The proportional derivative motor torque equation is computed through:

$$\tau_m = \mathbf{k}_p(\hat{\mathbf{q}} - \mathbf{q}) - \mathbf{k}_d\dot{\mathbf{q}}, \quad (7)$$

where \mathbf{k}_p and \mathbf{k}_d represent the gains, $\hat{\mathbf{q}}$ is the joint setpoint, \mathbf{q} is the joint position, and $\dot{\mathbf{q}}$ is the joint velocity.

The motor torque limit varies with velocity:

$$\tau_{\text{limit}} = \begin{cases} \tau_{\text{max}}, & |\dot{\mathbf{q}}| \leq \dot{\mathbf{q}}_{\tau_{\text{max}}} \\ \frac{\dot{\mathbf{q}}_{\text{max}} - |\dot{\mathbf{q}}|}{\dot{\mathbf{q}}_{\text{max}} - \dot{\mathbf{q}}_{\tau_{\text{max}}}} \cdot \tau_{\text{max}}, & \dot{\mathbf{q}}_{\tau_{\text{max}}} < |\dot{\mathbf{q}}| \leq \dot{\mathbf{q}}_{\text{max}} \\ 0, & |\dot{\mathbf{q}}| > \dot{\mathbf{q}}_{\text{max}} \end{cases} \quad (8)$$

τ_{limit} comprises a constant torque limit, τ_{max} , for braking and low velocities, and a linear reduction in available torque beyond a specific velocity, $\dot{\mathbf{q}}_{\tau_{\text{max}}}$. This linear limit reaches zero torque at the velocity $\dot{\mathbf{q}}_{\text{max}}$. For example, the sysIDed relationship for Dynamixel XC330 is illustrated in Figure 13.

The joint torque is then calculated by applying torque limits to τ_m and subtracting the frictional forces τ_f :

$$\tau = \text{clamp}_{[-\tau_{\text{limit}}, \tau_{\text{limit}}]}(\tau_m) - \tau_f, \quad (9)$$

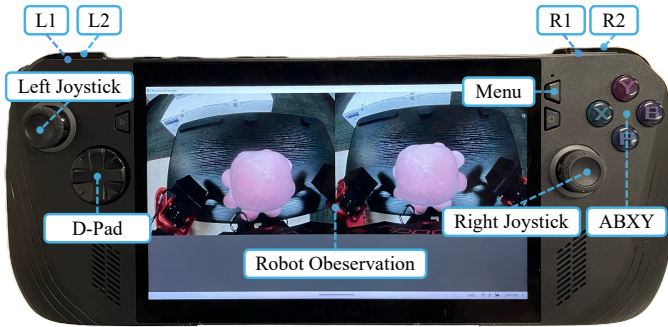


Figure 14: **Remote Controller Layout.** We show the button and axis layout on ROG Ally X.

Table V: Pupperteering Button and Axis Mapping

Button or Axis ^(a)	Effect
Menu	Toggle teleoperation / Mark episode start or end during data collection
Left Joystick \updownarrow	Walk forward or backward along the x-axis
Left Joystick \leftrightarrow	Walk leftward or rightward along the y-axis
Right Joystick \updownarrow	Stand up or squat down
Right Joystick \leftrightarrow	Turn clockwise or counterclockwise around the z-axis
D-Pad \updownarrow	Lean with the waist roll joint
D-Pad \leftrightarrow	Twist with the waist yaw joint
Y and A	Look up or down with the neck pitch joint
X and B	Look left or right with the neck yaw joint
L1	Hold to run the bimanual DP and release to end.
R1	Hold to run the full-body DP and run to end.
L2	Hold to run the wagon pushing policy and release to end.
R2	Hold to run the cuddling policy and release to end.

^(a) This mapping is compatible with various remote controllers and has been tested on the ROG Ally X and Steam Deck. The remaining buttons can be assigned to additional skills based on user preference.

where τ_f follows the joint passive force model in MuJoCo [45], which is characterized by three parameters: damping, armature, and friction loss. The sysIDed parameters for various Dynamixel motors are presented in Table IV.

H. Pupperteering Mapping

Figure 14 illustrates the remote controller layout to teleoperate ToddlerBot, with button and axis mappings detailed in Table V. During teleoperation, the human operator sends velocity commands to the walking policy and determines the timing for skill transitions. The same mapping was used for Steam Deck and ROG Ally X.

I. Reinforcement Learning Details

The RL implementation leverages MuJoCo XLA [45] and Brax [11]. We train the policy using PPO [40] with hyperparameters listed in Table VI. Inspired by prior work [15, 16], our reward function is shaped by three categories of reward terms as detailed in Table VII. Domain randomization is applied to body mass, geometry friction, and all parameters of the actuation model listed in Table IV. Full implementation details are available in our open-source codebase. During inference, the RL policy runs on the CPU of Jetson Orin NX 16GB, achieving a 50 Hz control loop while leaving the GPU available for other policies and models.

Table VI: Hyperparameters for PPO Training.

Parameter	Value
Policy hidden layer sizes	(512, 256, 128)
Value hidden layer sizes	(512, 256, 128)
Number of timesteps	3×10^8
Number of environments	1024
Episode length	1000
Unroll length	20
Batch size	256
Number of minibatches	4
Number of updates per batch	4
Discounting factor	0.97
Learning rate	0.0001
Entropy cost	0.0005
Clipping epsilon	0.2

Table VII: Reward Shaping for PPO Training.

Imitation Term	Value
Torso quaternion	1.0
Linear velocity (XY)	5.0
Linear velocity (Z)	1.0
Angular velocity (XY)	2.0
Angular velocity (Z)	5.0
Leg motor position	5.0
Feet contact	1.0
Regularization Term	
Feet air time	500.0
Feet clearance	0.05
Feet distance	1.0
Feet slip	0.05
Align with the ground	1.0
Stand still	1.0
Torso roll	0.5
Torso pitch	0.5
Collision	0.1
Leg action rate	0.05
Leg action acceleration	0.05
Motor torque	0.01
Energy	0.05
Survival Term	
Survival	10.0

J. Diffusion Policy Details

The diffusion policy processes a cropped and downsampled 96×96 RGB image, which is encoded by a ResNet [18] pretrained on ImageNet [7] to extract visual features. Both leader and follower joint angles are downsampled to 10 Hz for training, where the leader joint angles serve as actions and the follower as observations. To prevent motor overload during data collection, the upper body motors use low proportional gains, allowing modulation of the manipulation force. This behavior is embedded in the discrepancy between leader and follower joint angles, which the policy ultimately learns.

The model is trained with 100 diffusion steps. During inference, the trained model runs directly on the Jetson Orin NX 16GB with 3 DDPM steps, which are sufficient for satisfactory results. With 300M parameters, inference latency remains under 0.1 s on the GPU, ensuring smooth execution at 10 Hz without stuttering. Each inference yields a 16-step prediction; the first 3 actions are discarded to compensate for latency [4], and the next 5 actions are executed.

